Phase diagrams of Ce_2Pd_2In intermetallic compound

Author: P. Král [1]
Supervisor: J. Prchal [1]
Co-authors: J. Kaštil [2], M. Klicpera [1], P. Doležal [1]

[1]*Charles University, Faculty of Mathematics and Physics, Department of Condensed Matter Physics, Ke Karlovu 5, 121 16, Prague 2, Czech Republic*
[2]*Institute of Physics Czech Academy of Sciences, Na Slovance 1999/2, 182 21, Prague 8, Czech Republic*

Thanks to the specific electronic structure the rare earth-based compounds, especially those containing Yb, Ce or Eu, often exhibit exceptional magnetic properties. In our study we have focused on cerium-based compound Ce_2Pd_2In belonging to the family of R_2T_2X compounds crystallizing in tetragonal Mo_2FeB_2-type structure. Previous studies revealed presence of two magnetic phase transitions ($T_C \approx$ 4.1 K and $T_N \approx$ 4.5 K) and strong dependence of magnetic ground state on the changes of chemical composition.

We present the pressure-temperature phase diagrams both for hydrostatic and uniaxial pressure. Hydrostatic pressure acts in the same way on the whole lattice, while the uniaxial one allows to act solely in the chosen direction. The results are put into context with temperature evolution of crystal lattice investigated by low temperature X-ray diffraction. Based on these results, hydrostatic pressure is supposed to act more on the *a*-parameter, which leads to approaching of atoms in the basal plane, affecting the exchange interactions in the system and preference antiferromagnetic phase over the ferromagnetic one. On the other hand, the uniaxial pressure acts on the parameter *c* showing no significant effect on the temperatures of phase transition.

Introduction

Study of rare earth element-based compounds is in foreground of interest of condensed matter physics. Especially compounds containing Yb, Ce or Eu often exhibit interesting behavior such as non-integer valence or valence fluctuations [1, 2]. These are the well-known phenomena that are intensively studied both experimentally and theoretically [3-5]. The changes of valence can be accompanied for example with the onset of magnetism (or with its suppression) or with structure transitions (because the valence relates to the effective atomic radius).

In frame of the master thesis, we focused on Ce_2Pd_2In compound. Cerium-based intermetallic compounds attract much attention due to their anomalous physical behavior. It is predominantly governed by interactions of Cerium 4*f* electrons with non-*f* electrons of atoms in their neighborhood. This phenomenon is called *f*-ligand hybridization. The *f*-ligand hybridization is known to be very sensitive to external factors like magnetic field, pressure or to changes in atomic surroundings caused by hydrogenation – insertion of hydrogen atoms [6]. The main method we used for affecting the physical properties of chosen compound is application of mechanical pressure.

This text is the part of master thesis Unconventional behavior of Ce and Yb based compounds induced by extreme pressure. The selection of obtained results is dedicated to study of field and pressure influence on magnetic state of Ce_2Pd_2In compound given into context with the results of low temperature X-ray diffraction.

The theoretical part is restricted to the description of magnetic interactions in the system and of mechanical pressure. In experimental part, the extraordinary methods concerning application of mechanical pressure are described. Studied compound and its previously observed properties are summarized in Previous results. In the part Results, the most important new results are presented and finally discussed in Discussion.

Theoretical background

Magnetism [7]

Magnetic properties of condensed matter are well described by quantum theory. Origin of magnetism in materials is in magnetic moments of the magnetic ions present in the sample, the interactions between magnetic moments and in the interaction of the localized 4*f* electrons with the crystal field.

Magnetic moments in the matter can interact with each other and their interaction can lead to the long-range magnetic ordered state. There are two main types of interactions – the magnetic dipole interaction and the exchange interaction. Magnetic dipole interaction is very weak, and it can lead to magnetic ordered state only in very low temperatures (order of mK).

The second type is the exchange interaction. The Hamiltonian of the exchange interaction can be expressed according to the Heisenberg model as

$$\hat{\mathrm{H}}_{\mathrm{ex}} = -\frac{1}{2}\sum_{i,j} J_{ij}\hat{S}_i\hat{S}_j \,, \tag{1}$$

where J_{ij} stands for the exchange integral, describing the interaction between spins of two electrons i and j.

Exchange interactions can be divided into two groups.

First of them is the direct exchange interaction, which is typical for *d*-elements, light 5*f*-elements and their intermetallic compounds with sufficient overlap of appropriate wave functions of neighboring atoms with magnetic moment.

The second option is the indirect exchange interaction. In this case, the interaction between ions with magnetic moments is mediated by interaction with valence states of non-magnetic ligands – super-exchange (it prevails for example for some oxides of transition metals), or by conduction electrons – the RKKY (Ruderman-Kittel-Kasuya-Yoshida) interaction. In case of RKKY interaction, the localized magnetic moment polarizes conduction electrons in its vicinity and the information can be transferred

over the long distance. This interaction is typical for 4*f*-metals and 4*f*-intermetallics. The RKKY exchange integral can be written as

$$J_{RKKY} \propto \frac{\cos(2k_F r)}{r^3}. \tag{2}$$

All of these interactions are schematically shown in following Figure 1.

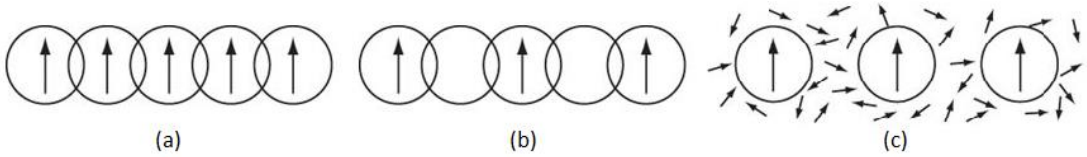

Figure 1: Magnetic exchange interactions: (a) Direct exchange, (b) Indirect Super-exchange, (c) Indirect RKKY interaction. Picture taken from [7]

Above mentioned interactions are affecting magnetic moments of atoms in the matter. It depends on many factors, if these interactions cause the magnetic order. Against them act for example thermal fluctuations of spin mean values. On the other hand, magnetic order is energy efficient.

In terms of basic types of order states, we can name ferromagnetism, antiferromagnetism or ferrimagnetism.

Ferromagnetic materials exhibit non-zero (so-called spontaneous) magnetic moment even without application of external magnetic field for temperatures below Curie temperature T_C. This temperature separates unordered paramagnetic phase for $T > T_c$ and ordered ferromagnetic state for $T < T_c$.

In the simplest case of antiferromagnetism, there are two ferromagnetic sublattices oriented antiparallel to each other, the exchange integral is negative. The magnitude of magnetic moments in each sublattice is the same. That's why the total magnetic moment of the bulk is zero. For such materials the temperature of ordering is called Néel temperature T_N.

Ferrimagnetism is the special case of previous (antiferromagnetism) with the difference that the magnitudes of moments in different sublattices are not equal in ferrimagnetic materials. The resulting spontaneous magnetic moment is non-zero. Ferrimagnetism occurs for example in materials containing two elements with different non-zero magnetic moments.

Mechanical pressure [9]

Magnetic interactions between magnetic moments in the condensed matter also depend on the distances between the magnetic atoms. There are several options how to affect the interatomic distances, namely by the temperature (due to the thermal expansion), by chemical substitution (replacement of one element with another one with different effective volume) or by external mechanical pressure. The advantage of the latter one compared to the chemical substitution lies in studying the same sample for the whole experiment. The substitution means using of different sample, i.e. matter with different chemical properties and also the electronic structure of the substituted compound. Another disadvantage is the fact that it is necessary to prepare several samples with given composition. Using the pressure allows us to avoid optimization process of preparation of samples with the new composition if only the change of interatomic distances is required. The temperature, on the other hand, changes neither the chemical nor the electronic structure, but it affects the degree of occupation of quantum states in studied compound.

Mechanical pressure is generally described as the force F acting on the surface S.

$$p = \frac{F}{S}. \tag{3}$$

For the accurate description of the pressure the stress tensor $\boldsymbol{\sigma}_{ij}$ is introduced, in cartesian coordinates the form is as following

$$\boldsymbol{\sigma} = \begin{pmatrix} \sigma_{11} & \sigma_{12} & \sigma_{13} \\ \sigma_{21} & \sigma_{22} & \sigma_{23} \\ \sigma_{31} & \sigma_{32} & \sigma_{33} \end{pmatrix}. \tag{4}$$

Diagonal components $\boldsymbol{\sigma}_{ii}$ stand for the direct stress in three orthogonal directions, while the non-diagonal elements represent the shear stress. Direct stress is normal to the surface and it tends to a volume change. The shear stress results in deformation of the sample shape without a volume change. Stress tensor is generally defined in every time and space point and the time and space dependent pressure can be defined as

$$p(\boldsymbol{r}, t) = -\frac{1}{3}\big(\sigma_{11}(\boldsymbol{r}, t) + \sigma_{22}(\boldsymbol{r}, t) + \sigma_{33}(\boldsymbol{r}, t)\big). \tag{5}$$

In a special case, when the non-diagonal elements of the stress tensor are zero and the diagonal components are equal (case of isotropic stress), we can introduce the hydrostatic pressure by formula

$$p(\boldsymbol{r},t) = -\sigma_{11} = -\sigma_{22} = -\sigma_{33}\,. \tag{6}$$

Mechanical hydrostatic pressure applied on the sample leads to changes in sample properties. As mentioned above, the main reason is the fact, that pressure affects the interatomic distances in the matter. The lattice parameters can be increased or decreased, but the resulting volume decreases. The change in volume can be described by the isothermal compressibility

$$\kappa = -\frac{1}{V}\left(\frac{\mathrm{d}V}{\mathrm{d}p}\right)_T. \tag{7}$$

Compressibility of the material is in general decreasing with increasing the pressure ($\kappa \sim V^{5/3}$) while the volume decreases with increasing pressure. The same impact has the pressure on the number of electrons on Fermi level ($N(E_F) \sim V^{2/3}$), while the Fermi energy is decreasing ($E_F \sim V^{-2/3}$).

Mechanical pressure has also impact on electronic structure of the material. Increased pressure leads to enhancement of the overlap of atomic wave functions accompanied by the increase of values of overlap integrals. The electron bands are getting wider, the energy gaps can be reduced (it can affect other material properties – optical, electric conductivity and so on) at enhanced pressure. Pressure can also lead to the delocalization of electrons, also the binding character can be influenced (from ionic through covalent to metal bond with increasing the pressure).

Decrease of interatomic distances induced by pressure can affect the exchange interactions. Changes in the value of exchange integral J_{ij} have the impact on ordering temperatures and cause their shift. In compounds where RKKY interaction prevails, also the type of magnetic order can be affected because of the change in the sign of the exchange integral.

Application of pressure on superconducting materials usually leads to lowering of the transition temperature. This phenomenon is used in the secondary manometers for

pressure determination in the pressure cell. As an example, the pressure dependence of superconducting transition in Pb is given as [10]

$$T_C(p) = T_C(0) - 0.0405p(\text{kbar}), \tag{8}$$

where $T_C(0) = 7.19\,\text{K}$ stands for the Pb superconducting transition in ambient pressure.

Experimental methods – High pressure experiments

Several types of pressure cells were used for application of the mechanical pressure. The choice depends on the physical property we intend to study or on the device used for measuring – it limits the suitable dimensions of the cell.

Hydrostatic double layer pressure cell

A double layer cylindrical pressure cell made of CuBe (outer layer) and NiCrAl (inner layer) with nominal pressure range up to 3 GPa [11] was used for measurement of electrical resistivity and AC magnetic susceptibility, both at the same time (in order to ensure the same conditions) under high pressure.

The sample of suitable dimensions is fixed to the thin paper by GE varnish. Four gold wires were used for four-point configuration method of electrical resistivity measurement to eliminate the influence of resistance of wires. Micro-welding was used to make electrical contacts and also the silver paste was used to reinforce them because they are strained a lot during both preparation and duration of experiment. Then the sample was put into the system of coils with the inner diameter of 1.66 mm. This system consists of the excitation (200 turns) and detection (signal) coil with the compensation coil (50 + 50 turns) winded in opposite direction. The measured signal contains the induced voltage caused by the magnetic signal from the sample (detection part) with directly subtracted signal from the environment (compensation part without sample). Four resistivity wires were connected to the plug with the silver paste DuPont and the connection of four wires from coils and also manganin wire to the plug was realized by soldering. Thermally stabilized manganin wire serves for determination of the pressure at room temperature. For particular manganin wire the dependence of its resistance on the pressure can be described as

$$R(T,p) = R(T,0)(1 + \alpha(T)p), \tag{9}$$

where α is the pressure coefficient of resistance of manganin which was in our case α = 0.00246 at room temperature. The pressure difference between the room- and the lowest measured temperature inside the pressure cell is $\Delta p \approx 0.3$ GPa and it remains similar all over the used range of pressures.

The whole measurement assembly is put inside the Teflon cell with the length of 21 mm and diameter 4 mm (outer) and 3 mm (inner).

All parts of the pressure cell are shown in the following Figure 2.

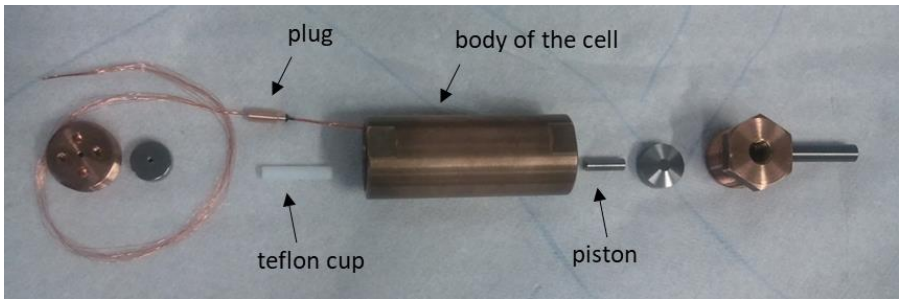

Figure 2: CuBe/NiCrAl double layer cylindrical piston hydrostatic pressure cell. Picture taken from [12]

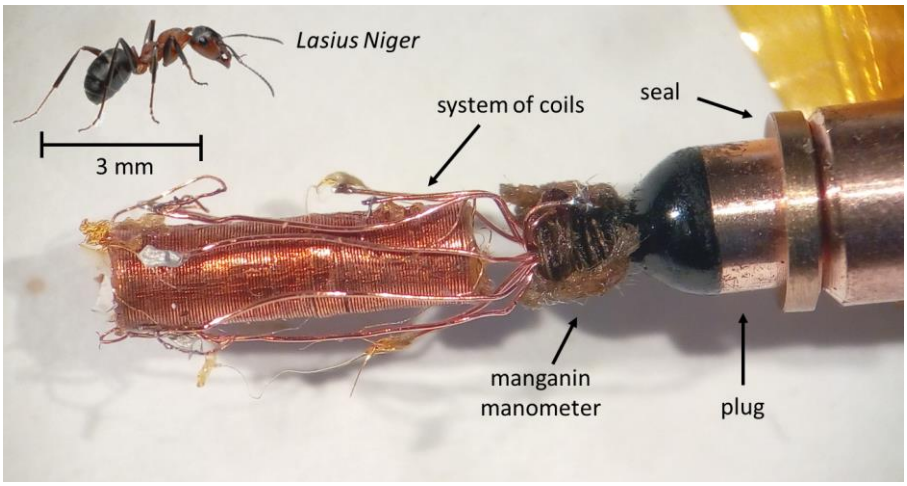

Figure 3: Preparation of the sample for measurement in pressure cell shown in Figure 2. For the better idea of size, the picture of an ant [13] is added to the figure

As a pressure-transmitting medium Daphne oils 7474 and 7575 were used [14,15]. These media ensure the equal distribution of pressure (hydrostaticity) within the sample space of the pressure cell.

Hydrostatic pressure cell for magnetization measurement

The magnetization of the sample was measured in the CuBe hydrostatic pressure cell designed by Ing. J. Kamarád, CSc. (Institute of Physics, Academy of Sciences, [16]). It allows us to measure the magnetization in SQUID magnetometer MPMS for pressures up to 1 GPa. The cell is shown in the Figure 4. The sample is fixed by GE varnish in the chamber. As the pressure transmitting medium, Daphne oil 7373 was used [17]. The space filled by the medium is sealed by the series of seal rings. Finally,

the pressure is realized by the piston pushed by tightening the screw. This pressure cell allows us to measure the pressure at low temperatures. The applied pressure is approximately settled at room temperature from the known number of turns of the screw and the exact value is determined according to the superconducting transition of lead (see (8)).

Figure 4: CuBe hydrostatic pressure cell for magnetization measurement

The uniaxial pressure cell

In order to apply the uniaxial pressure on the studied sample, the CuBe uniaxial pressure cell similar to the one mentioned in previous paragraph was used (Figure 4) [18]. This pressure cell allows to measure the magnetization in MPMS. Contrary to the hydrostatic pressure described in the previous paragraph, no exchange medium should be used as the pressure is uniaxial by wish in this case. Pressure is determined directly from the definition (1.32), where F stands for the force, which is given by number of screw turns – in the cell, there is the spring with defined stiffness, and S is the area of the sample. For this kind of experiment, the sample with dimensions approx. 1×1 mm and the thickness max. 200 μm is used.

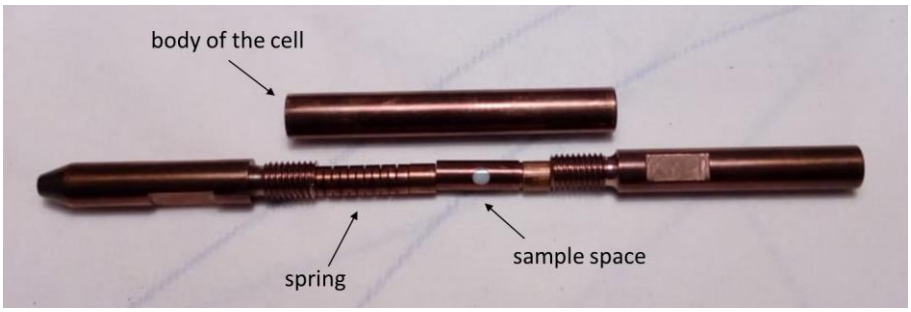

Figure 5: CuBe uniaxial pressure cell

Previous results and motivation

Numerous 2:1:2 intermetallic compounds belonging to R_2T_2X family (T stands for the transition metal, X for p-metal) crystallizing in tetragonal Mo_2FeB_2-type structure exist both for R = lanthanides and actinides [19]. This structure type is the ternary derivative of U_3Si_2 (space group 127: P4/*mbm*). This is a good opportunity to compare the appearing magnetism in 4*f* intermetallics with magnetism related to 5*f* states in actinide-based compounds. Materials based on actinides (U, Np, Pu) exhibit crossover from antiferromagnetic order to weak Pauli paramagnetism, when the hybridization between 5*f* states and ligand states gets stronger. On the other hand, 4*f*-element based compounds are mostly antiferromagnetic. The most typical interaction responsible for magnetic order in the latter case is RKKY interaction.

Interesting magnetic properties of such materials are related to the crystal structure. As it is shown in Figure 6, the lattice is formed by planes consisting of the rare earth elements with possible non-zero magnetic moment alternated by non-magnetic planes containing other elements. The rare earth atoms are forming triangular motif, which can, depending on the character of exchange interaction, bring the geometrical frustration into the system. This is equivalent to the two-dimensional Shastry-Sutherland lattice [20].

Ce_2Pd_2In

Discovery of U_2T_2X compounds (T stands for transition metal, X for In or Sn) crystallizing in the Mo_2FeB_2-type structure led to synthesis and characterization of the Ce counterparts. Several compounds with the formula Ce_2T_2X have been investigated and some of them exhibit interesting properties such as heavy fermion or Kondo behavior [21].

Depending on the character of *d*-band of transition metal T in Ce_2T_2In the compounds exhibit well-localized magnetism (Ce_2Cu_2In, Ce_2Pd_2In and Ce_2Au_2In) or valence fluctuations (T = Ni, Rh) [22,23]. For Ce_2Pd_2X (X = In, Sn, Pb), there was observed magnetic ordering at low temperatures [21]. Among the group of R_2Pd_2In compounds, the Ce-based one exhibits the most interesting magnetic behavior. It reaches the ferromagnetic ground state below 4.1 K through an intermediate antiferromagnetic

phase [24-26]. Similar magnetic properties were observed in Ce_2Pd_2Sn, which reaches the ferromagnetic grounds state below 2.2 K also through an antiferromagnetic interphase [27].

Physical, especially magnetic, properties are strongly dependent on the interatomic distances in crystal lattice. In previous studies, the so called chemical pressure was applied in sense of changing the stoichiometry or by hydrogenation.

Hydrogen content up to 1.5 in $Ce_2Pd_2InH_x$ leads to ferromagnetic ground state, while for larger amount, up to x = 2.5, the compound orders antiferromagnetically. There were nevertheless CeH_2 and CePdIn impurities present in the sample for higher hydrogen content. With increasing of H content, almost linear and nearly isotropic expansion in both of lattice directions a and c was observed. Such behavior suggests that hydrogen atoms randomly occupy interstitial positions [6].

Magnetic ground state of Ce_2Pd_2In compound was also found to be very sensitive to the off-stoichiometry [28]. The excess of Ce at the expense of In in $Ce_{2+x}Pd_{1.85}In_{1-x}$ leads to ferromagnetic ground state, while the excess of Pd in $Ce_{1.95}Pd_{2+2x}In_{1-x}$ results in incommensurate sinusoidal modulated type of antiferromagnetism, which can be described by propagation vector $k \approx [0.22,0,0]$. The neutron diffraction data showed that the magnetic moments are in both cases (Pd-rich, Ce-rich composition) oriented parallel to the *c*-axis. The observed change in the magnetic ground state may be rationalized by the oscillating nature of RKKY exchange interaction. Both phase transitions are present in the case of accurate stoichiometry [24].

Another way, how to affect the interatomic distances, is application of mechanical pressure. As the most common exchange interaction in rare earth-based compounds is the RKKY interaction (for which the sign depends on the distance between magnetic ions), pressure poses the way, how to influence magnetic properties. Another feature that can be affected by pressure is the valence state of the rare earth element.

All of above mentioned results were obtained for polycrystalline samples. M. Klicpera et al. [24] dealt with studying of magnetic properties of single crystals with stoichiometry on slightly Pd-rich side. Investigation by means of X-ray diffraction, magnetization, specific heat and electrical resistivity was carried out and confirmed

the presence of two magnetic transitions. The ground magnetic state of this compound is ferromagnetic. Around temperature 4.1 K it changes into antiferromagnetic and then, around 4.5 K, there is the second phase transition to the paramagnetic state. Measurements of magnetization were carried out with field orientation along three directions – [100], [110] and [001]. Results for field along the basal plane directions are almost identical. On the other hand, a relatively strong anisotropy was observed using the third mentioned field direction (field along *c*-axis). The *c*-axis was found as an easy-axis of magnetization. It is in good agreement with above mentioned result of neutron diffraction [28]. Effective magnetic moment was found to be $\mu_{eff} = 2.38\,\mu_B/\mathrm{Ce}$ (close to Ce^{3+} free ion $\mu_{eff} = 2.54\,\mu_B/\mathrm{Ce}$). Also the obtained saturated magnetic moment $2.16\,\mu_B/\mathrm{Ce}$ for magnetization easy axis *c* is close to the value for free Ce^{3+} ion moment of $2.14\,\mu_B/\mathrm{Ce}$. Lower values obtained in some previous studies for polycrystalline samples [28] were considered as the consequence of averaging of randomly oriented grains with high uniaxial anisotropy in [24]. For paramagnetic Curie temperature, two values were obtained as the consequence of anisotropy. Their difference $\Delta\theta_P \approx 62$ K can be used to calculate the uniaxial anisotropy energy $\Delta E_A = k_B \Delta\theta_P \approx 5.3$ meV. Results given by magnetization and heat capacity measurements were compared to the first principle calculations and reasonable agreement was obtained. The Sommerfeld coefficient of electronic specific heat was estimated, using results of electrical resistivity measurement, as $\gamma = 50$ mJ mol^{-1} K^{-2}. This value is not enhanced enough to indicate the compound as heavy fermion ($\gamma > 400$ mJ mol^{-1} K^{-2}). In terms of two phase transitions, curves $M/H\ (T)$ are discussed in dependence on magnetic field. For higher values of field, transitions become less distinguished and they merge around 0.1 T, when the saturation is achieved for H along c. Measurements of electrical resistivity showed the difference between curves with different current direction for temperatures below 250 K, over this temperature, the resistivity values become quite isotropic.

Results and discussion

X-ray powder diffraction

The X-ray powder diffraction was used for determination of the crystal structure of the studied compound. We verified, that Ce_2Pd_2In crystallizes in expected tetragonal Mo_2FeB_2-type structure of space group P4/*mbm* (space group number 127). Diffraction patterns were processed using the FullProf software developed in ILL. Crystal structure of Ce_2Pd_2In compound is shown in Figure 6, which was obtained using the Vesta software. The room temperature lattice parameters were found to be $a = 7.801(2)$ Å and $c = 3.919(1)$ Å.

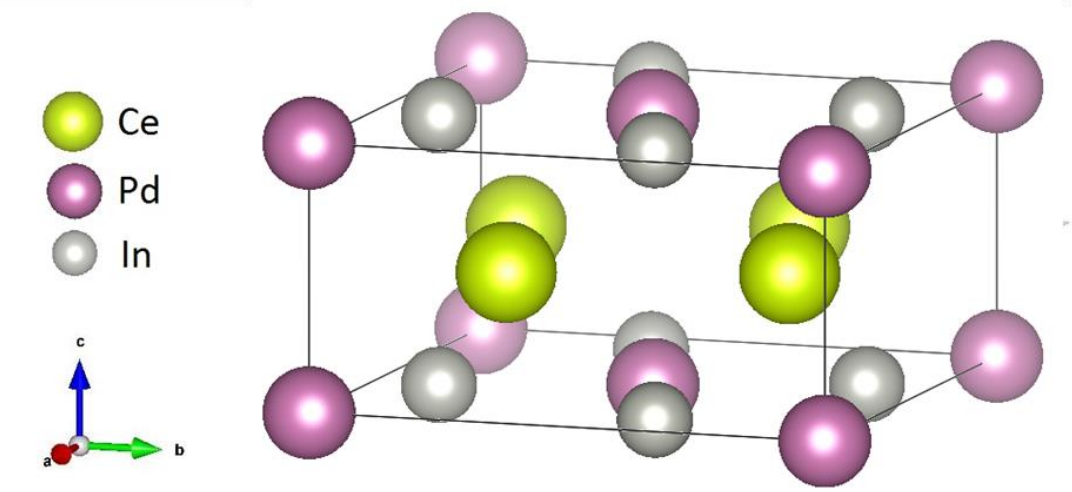

Figure 6: Crystal structure of Ce_2Pd_2In (tetragonal P4/*mbm*)

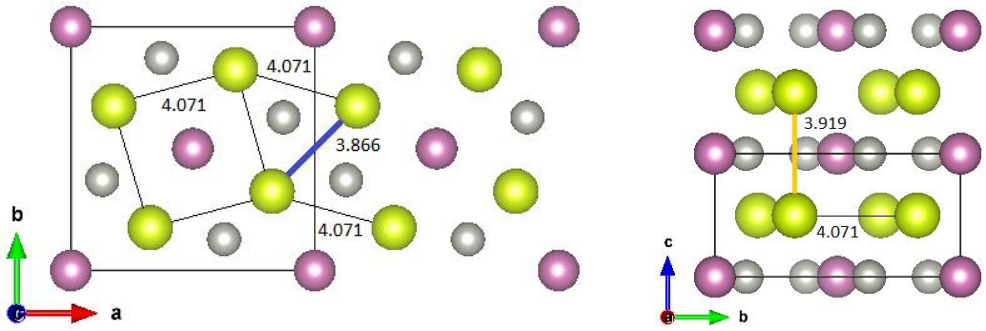

Figure 7: The position of magnetic nearest neighbors (Ce-Ce dimers) marked by the blue line (view along *c*) and of the second nearest neighbors – orange line (view along *a*). Distances (obtained at room temperature) are given in Å.

In combination with cryocooler, X-ray powder diffraction allowed us to investigate the temperature dependence of lattice parameters.

The results are summarized in Figure 8. Strong anisotropy of temperature evolution of the lattice parameters *a* and *c* was observed. While dimension of the longer basal lattice parameter *a* decreases with temperature, perpendicular *c*-parameter is getting longer, however the changes are approximately 3-times smaller compared to parameter *a*. Temperature evolution between 3.2 and 300 K is shown in Figure 8.

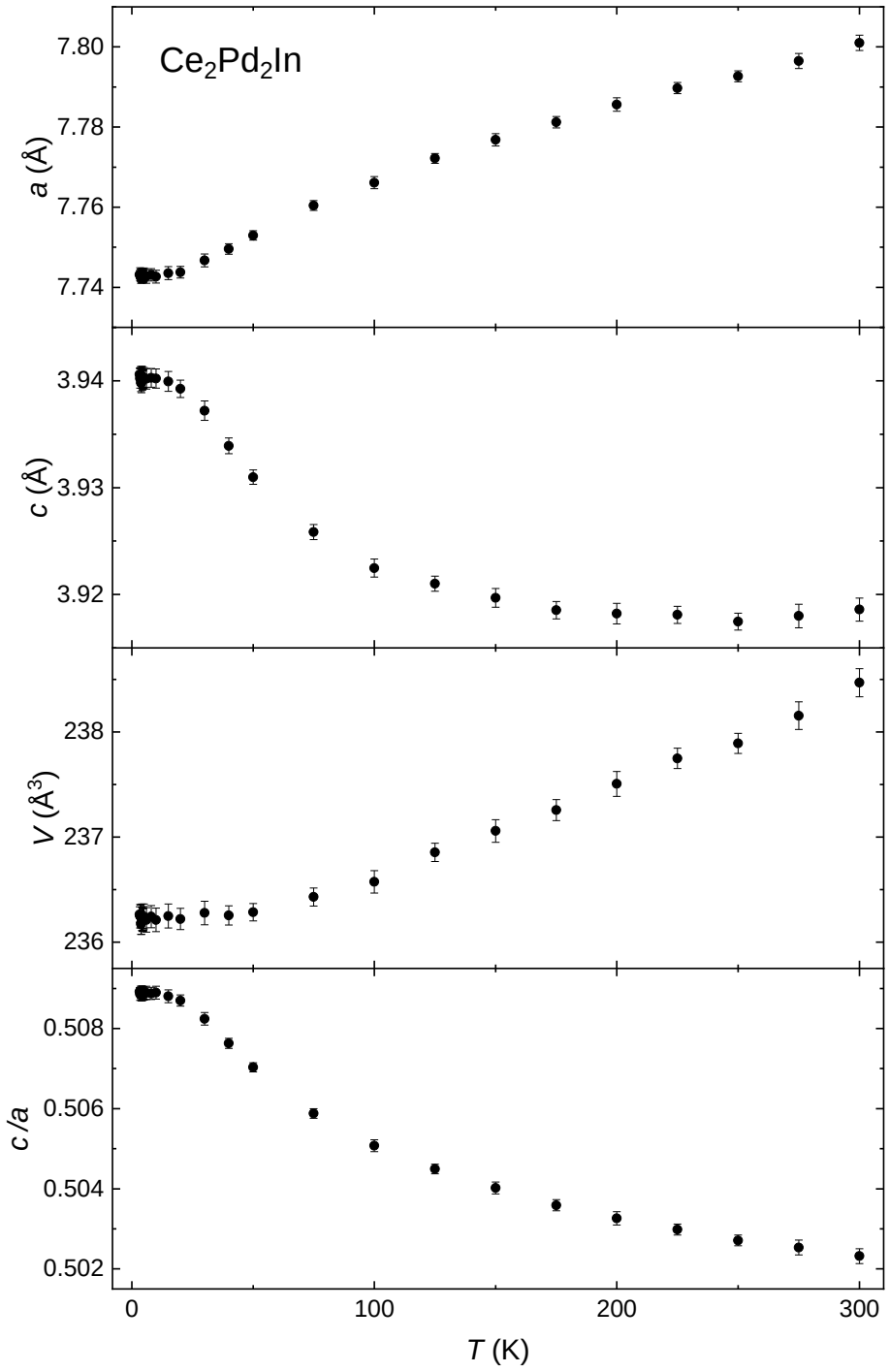

Figure 8: Temperature dependence of lattice parameters obtained by low temperature X-ray diffraction

From the measured low-T XRD data, we have also investigated the evolution of distance between the nearest magnetic ions – Ce in our case. At room temperature, the Ce ions lying in basal plane form a square motif formed by Ce dimers as it is shown in Figure 7. The Ce-Ce distance in these dimers is also the shortest Ce-Ce distance in the compound. The second nearest neighbor lies in another Ce plane sheet, the distance is thus equal to lattice parameter *c*. Because this parameter is increasing while temperature decreases, the distance is getting longer. On the other hand, lattice parameter *a* is decreasing with cooling, that's why Ce atoms within the particular plane are getting closer to each other.

Ambient pressure characterization

All experiments discussed below provide important physical information. Measured properties are also influenced by the presence of magnetic phase transitions. Figure 9 depicts the temperature region around them. We can see that both transitions are connected with some anomaly on the curve. Vertical lines correspond to the positions of transitions determined from the heat capacity data using the method of idealization of transition according to specific heat while maintaining the entropy (see below for more detailed explanation). Because of the second order of both transitions, the entropy of the system evolves continuously. Although the transition is not very clearly determined by the electrical resistivity curves, the transitions cause two significant breaks on the curves and also the inflex points below the breaks can be found using the derivative of the curve. Much more clear is the situation in AC magnetic susceptibility and on the magnetization data. Both of these physical properties exhibit the inflex point at the temperatures of phase transitions.

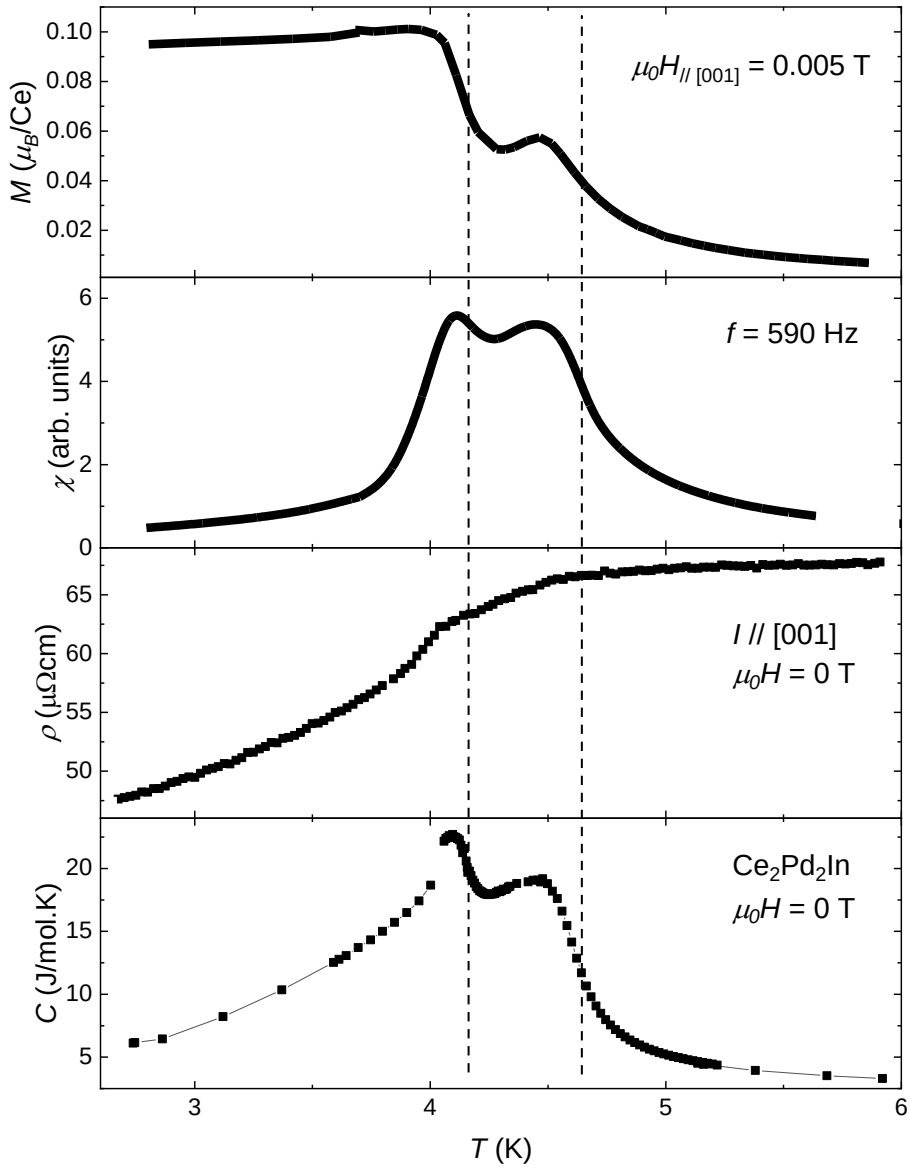

Figure 9: Magnetic phase transitions represented by anomalies in temperature evolution of several physical properties – magnetization, AC magnetic susceptibility, electrical resistivity and heat capacity, the vertical lines correspond to the temperatures of phase transitions determined from the heat capacity curves

DC magnetization

Magnetization was investigated in the temperature region between 2 K and 350 K with external magnetic field applied along two directions – along [110] and along the [001] direction. A strongly anisotropic behavior was observed. The *c*-axis was verified to be the easy axis of magnetization. Following figures summarize the magnetization data for both directions of external magnetic field.

In terms of the region around magnetic phase transitions, the measurement of temperature dependence of magnetization was carried out in zero field cooled (ZFC)

and field cooled (FC) regime for various values of external magnetic field, the results are summarized in Figure 10. All curves are flat at higher temperatures. When the temperature is approaching the transitions, the values start to grow, and the curvature appears on the dependences. Critical temperatures of phase transitions can be determined as the inflex points on the curves according to Figure 9 and it allows us to construct the $\mu_0 H - T$ phase diagrams shown in Figure 11. The fact that the FC and ZFC curves differ at low temperatures corresponding to the ferromagnetic state is the typical feature of ferromagnetic behavior. The origin of such behavior is in presence of magnetic domains. External magnetic field applied in case of FC curve plays the role in their orientation and that's why they tend to reach higher value of magnetization. In the second case, ZFC curves start from the state, where they are not oriented. This leads to the lower observed value of magnetization in the lowest temperatures. When applied external magnetic field is high enough, this effect does not play any role and both curves merge.

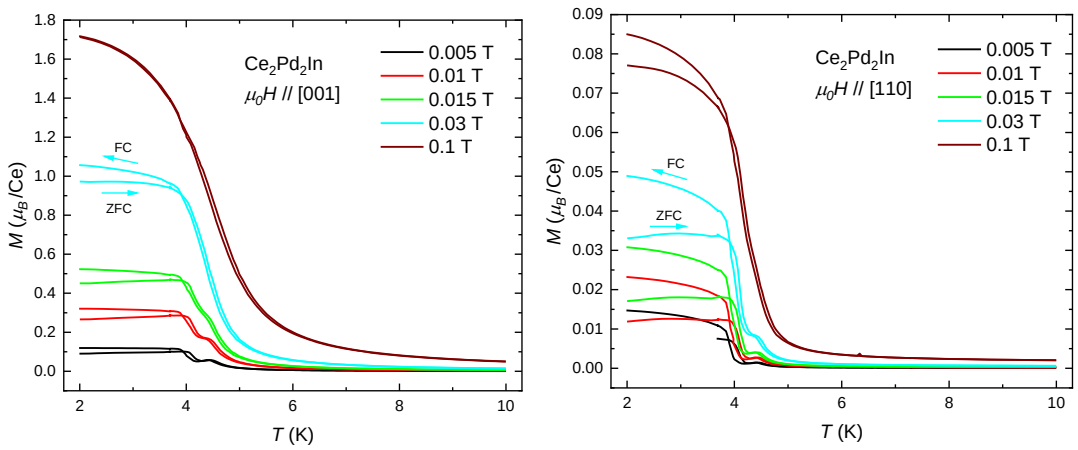

Figure 10: Temperature dependence of magnetization for various values of external magnetic field applied along [001] – the easy axis of magnetization (left figure) and along [110] direction (right figure)

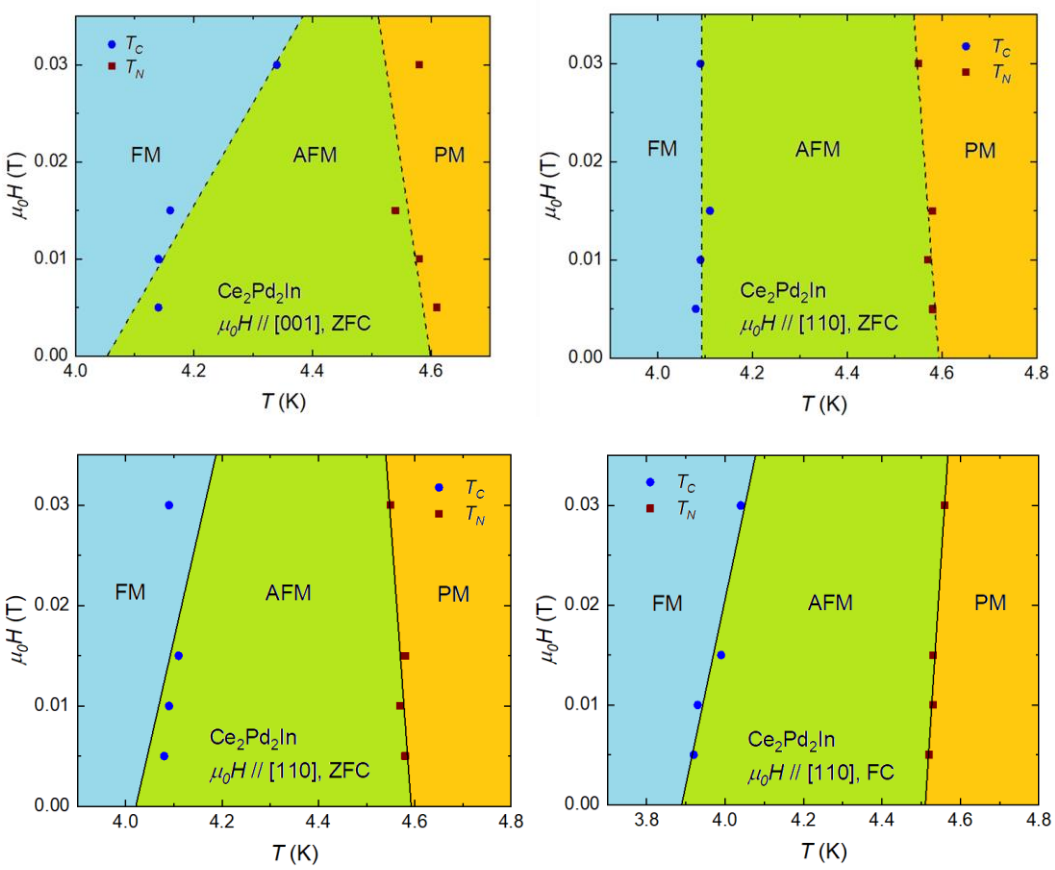

Figure 11: Phase diagrams of Ce_2Pd_2In ($\mu_0 H - T$), FM stands for the ferromagnetic, AFM for antiferromagnetic and PM for paramagnetic region, positions of phase transitions were determined from the magnetization data for both field directions and ZFC and FC regimes. Estimated points were fitted by linear curve to display the trend of evolution more clearly.

Application of hydrostatic pressure

Electrical resistivity

Electrical resistivity as well as the AC magnetic susceptibility discussed in the following subchapter were measured in the double layered CuBe/NiCrAl hydrostatic pressure cell. The resistivity curves in various values of pressure are presented in Figure 12. Shape of the resistivity curve is sensitive to applied pressure, significant minimum around temperature of 150 K is formed with increasing the pressure. The bump at around 70 K mentioned above in the ambient pressure case is present in all pressures, but it is shifted to lower temperatures. Also the minimum above the phase transitions is present in all pressure values. The residual resistivity is higher in higher pressures. The values of resistivity at 2 K as the lowest temperature measured in all pressures are shown in following Table 1.

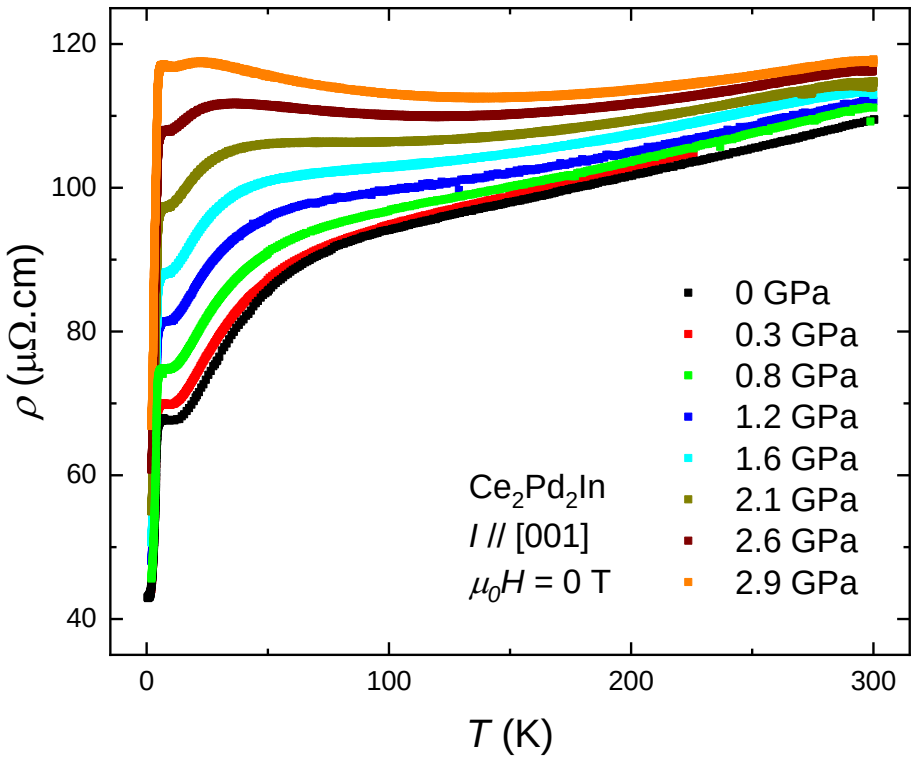

Figure 12: Electrical resistivity curves in pressure range between 0 GPa and 2.9 GPa and zero external magnetic field

Table 1: Resistivity obtained at 2 K for various values of applied hydrostatic pressure

p (GPa)	0	0.3	0.8	1.2	1.6	2.1	2.6	2.9
ρ_{2K} (μΩcm)	43(1)	44(1)	46(1)	48(1)	51(2)	55(2)	61(2)	67(2)

Following Figure 14 depicts the region around the phase transitions. The data are shown in the form of R_{10}/R, where R_{10} stands for the resistivity value at 10 K as the temperature lying above the transitions. In the graph there is shown the evolution of inflex point which is related to the magnetic phase transition. The real position of the transition is above this anomaly as it is discussed above. It is evident, that the antiferromagnetic transition is not affected much by the mechanical pressure. On the other hand, the ferromagnetic transition is shifted significantly to lower temperatures.

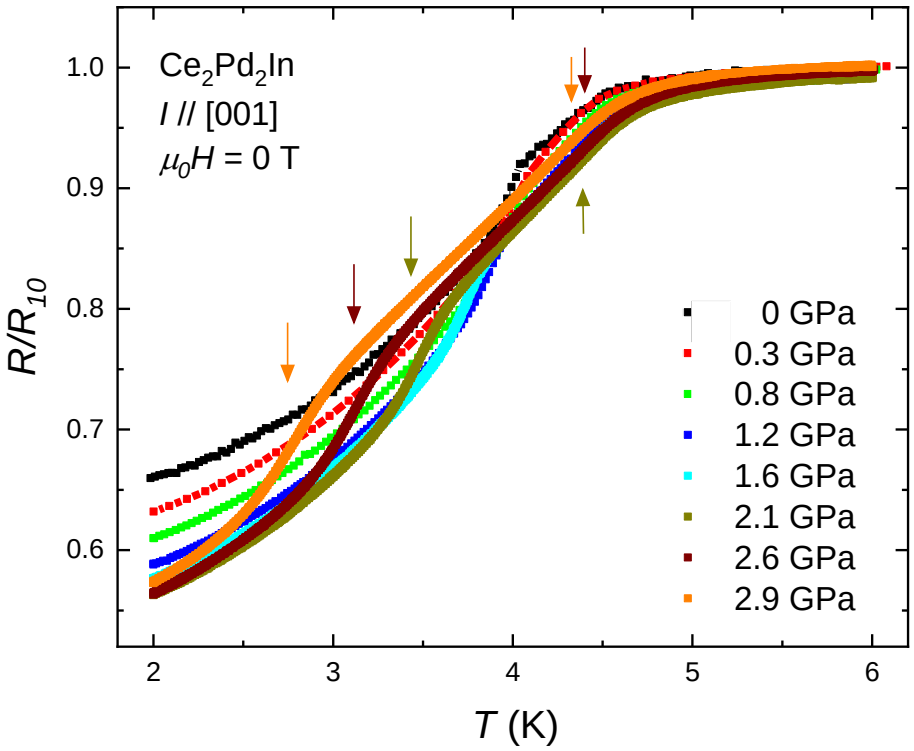

Figure 13: Electrical resistivity curves in pressure range between 0 GPa and 2.9 GPa and zero external magnetic field in the region around magnetic phase transitions

AC magnetic susceptibility

As it is has been mentioned already above, the AC magnetic susceptibility was measured also in the double layer pressure cell in pressures up to 3 GPa. We obtained very similar behavior as in the ambient pressure situation. Two maxima connected with the transitions appear on the curves of susceptibility. Also here the data for susceptibility amplitude and its real part overlap, similar to ambient pressure. According to Figure 9, the AC susceptibility data can be used for determination of the positions of phase transitions. In accordance with determination of the transition at ambient pressure we expect the transition appearing as the inflex points lying above two significant maxima appearing on the curves. The region around the transitions is shown in Figure 14. The arrows of particular colors correspond here to the critical temperatures obtained at various pressures.

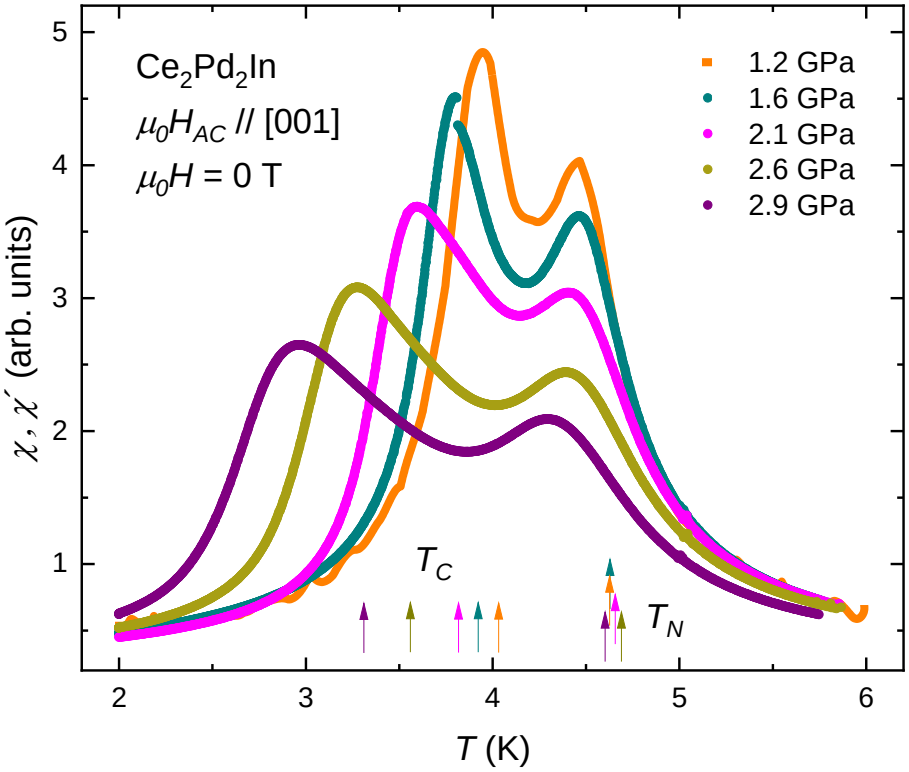

Figure 14: AC magnetic susceptibility (amplitude χ, real part χ') for various values of external mechanical pressure, the arrows show the positions of phase transitions (arrow colors correspond to the colors of the curves)

Magnetization

Magnetization was measured in CuBe pressure cell up to 1.1 GPa. As it is mentioned in Experimental methods, pressure was determined from the temperature of superconducting transition in Pb.

Following graph contain the magnetization curves measured at 2 K at several pressure points. We can clearly observed the pressure reduction of saturated magnetic moment probably caused by increase of magnetic fluctuations in agreement with pressure induced increase of residual resistivity ρ_R.

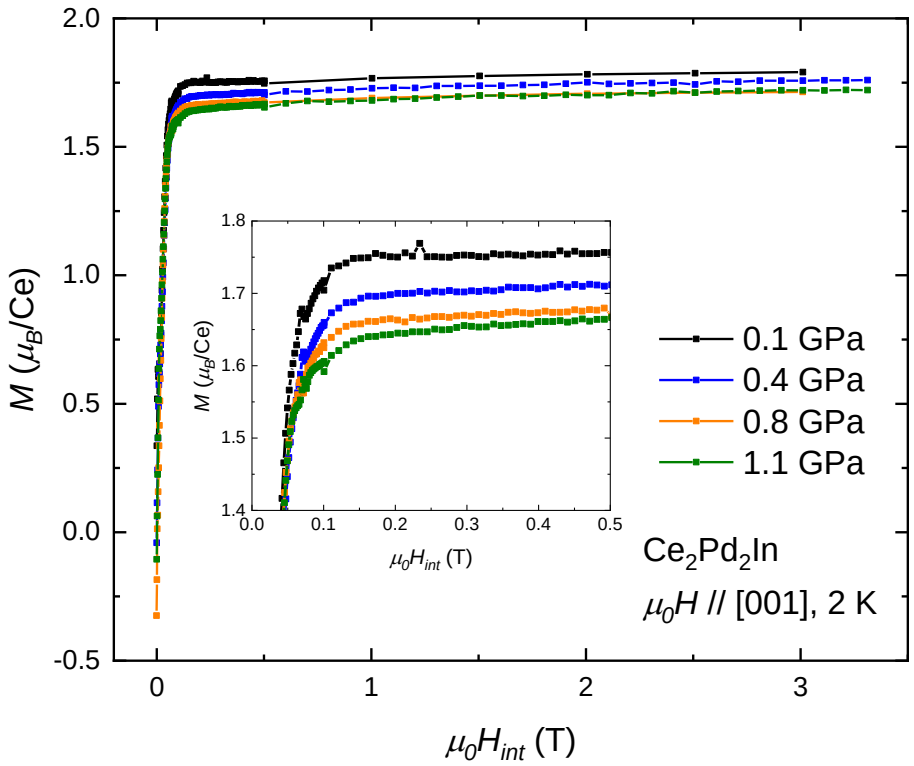

Figure 15: Magnetization curves measured at 2 K for various values of hydrostatic pressure, the colors are chosen with respect to the pressure values in the uniaxial pressure experiment discussed below

All experiments discussed in previous including measurement of electrical resistivity, AC magnetic susceptibility and DC magnetization under pressure provide the information about pressure evolution of the positions of both observed magnetic phase transitions. As it is already mentioned above, suitable for determination the critical temperatures are especially the magnetization measurements and the measurements of susceptibility. On both of these quantities, two inflex points can be found at temperatures of transitions. Determined positions allow us to construct the $p - T$ phase diagram shown in Figure 16. This diagram shows evolution of characteristic temperatures of both magnetic transitions (Curie temperature T_C for the ferromagnetic and Néel temperature T_N for antiferromagnetic one) in dependence on hydrostatic pressure. Applied pressure affects both phase transitions. We can see the systematic suppression of ferromagnetic phase, the antiferromagnetic phase remains to significantly lower temperature under applied pressure, while the temperature of antiferromagnetic transition is not affected a lot. For estimation of total suppression of the ferromagnetic state, the extension of the experiment to higher pressure range is needed. The estimation of required pressure is given in Figure 17 by the extrapolation of the pressure dependence of Curie temperature to the zero temperature. This way we

obtained $p_{T_C \to 0} \approx 5$ GPa. To confirm this estimation a higher pressure application is needed.

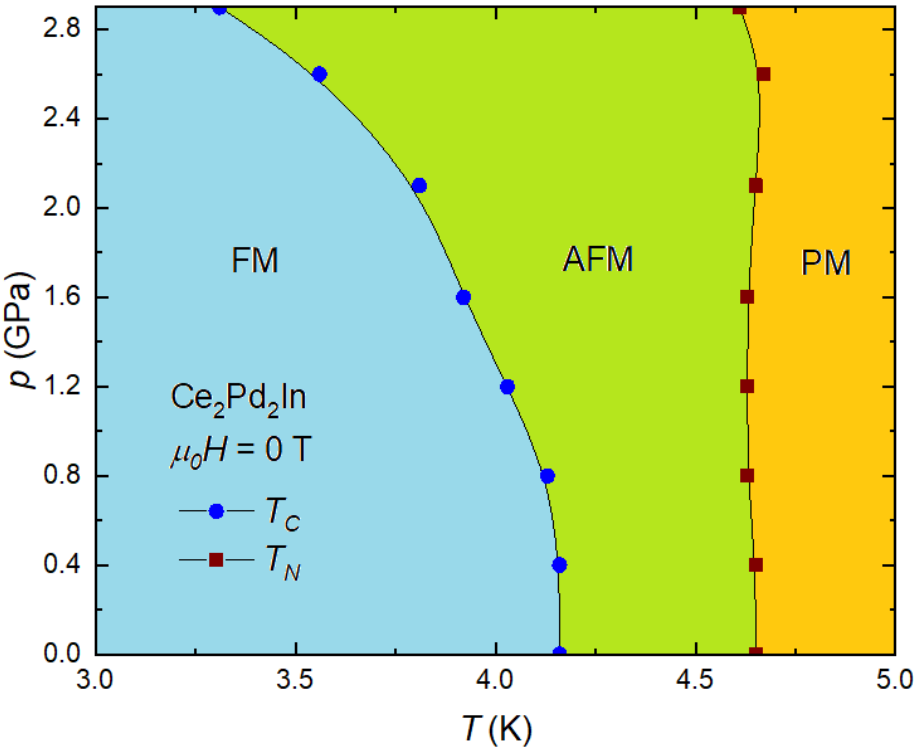

Figure 16: Phase diagram showing the evolution of critical temperatures of magnetic phase transitions in dependence on applied mechanical pressure

In following phase diagram, there is shown the extrapolation of the dependence of Curie temperature on applied pressure already mentioned above. It provides only the rough estimation of the pressure required for the total suppression of ferromagnetic state. In terms of the Néel temperature, no prediction can be done from measured data, because of the fact that until the highest measured pressure of 2.9 GPa, the changes of T_N is not significant.

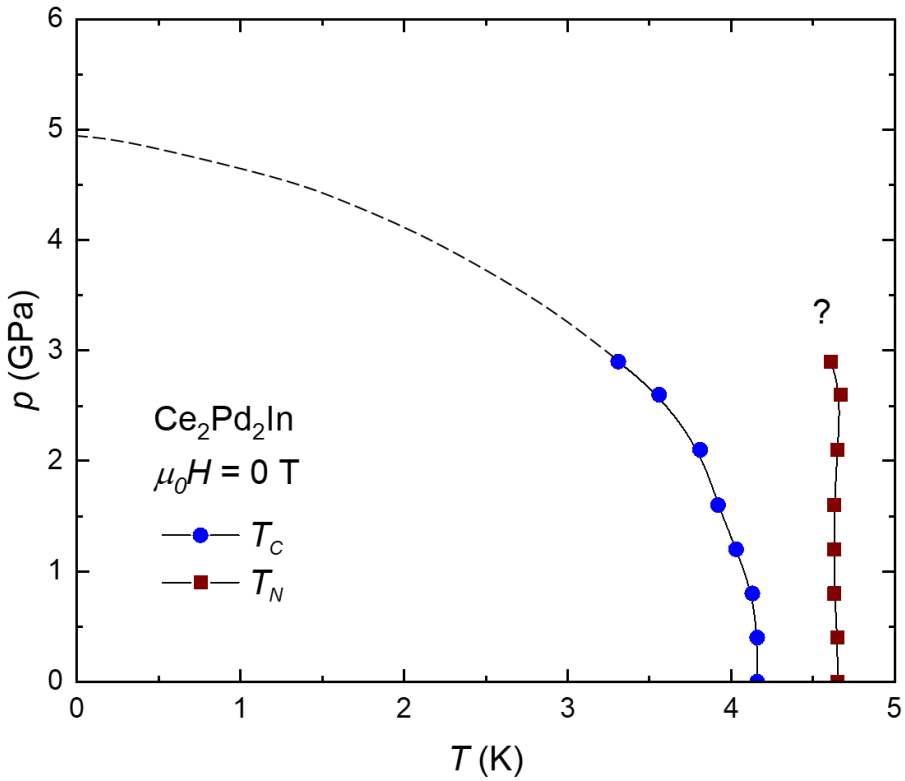

Figure 17: Extrapolation of $p - T$ phase diagram to $T_C = 0$

Application of uniaxial pressure

The uniaxial pressure was applied along the *c*-axis in CuBe uniaxial pressure cell, which allows us to measure the magnetization in MPMS. External magnetic field was applied along the easy axis of magnetization *c*.

Figure 18 contains magnetization data in dependence on temperature and applied pressure. These curves allow us to study positions of phase transitions (as the inflex points on the curves) and to construct $p_{uniaxial} - T$ phase diagrams as it is shown in Figure 19. When comparing the individual graphs one can see the saturation in the lowest temperature according to expectation from ambient pressure experiment. Here, the higher external magnetic field is applied, the higher saturated magnetization is reached. Magnetic field also affected the shape of the curves, for the highest 0.1 T field, it is very difficult to find the position of antiferromagnetic transition, the antiferromagnetic phase is being suppressed by field. This is well visible on the phase diagrams below these graphs.

On the other hand, the uniaxial pressure up to 0.5 GPa does not affect the shape of the curves significantly. Also the positions of phase transitions do not change significantly

under applied pressure. However, the slight tendency to systematic increase of the Curie temperature can be seen.

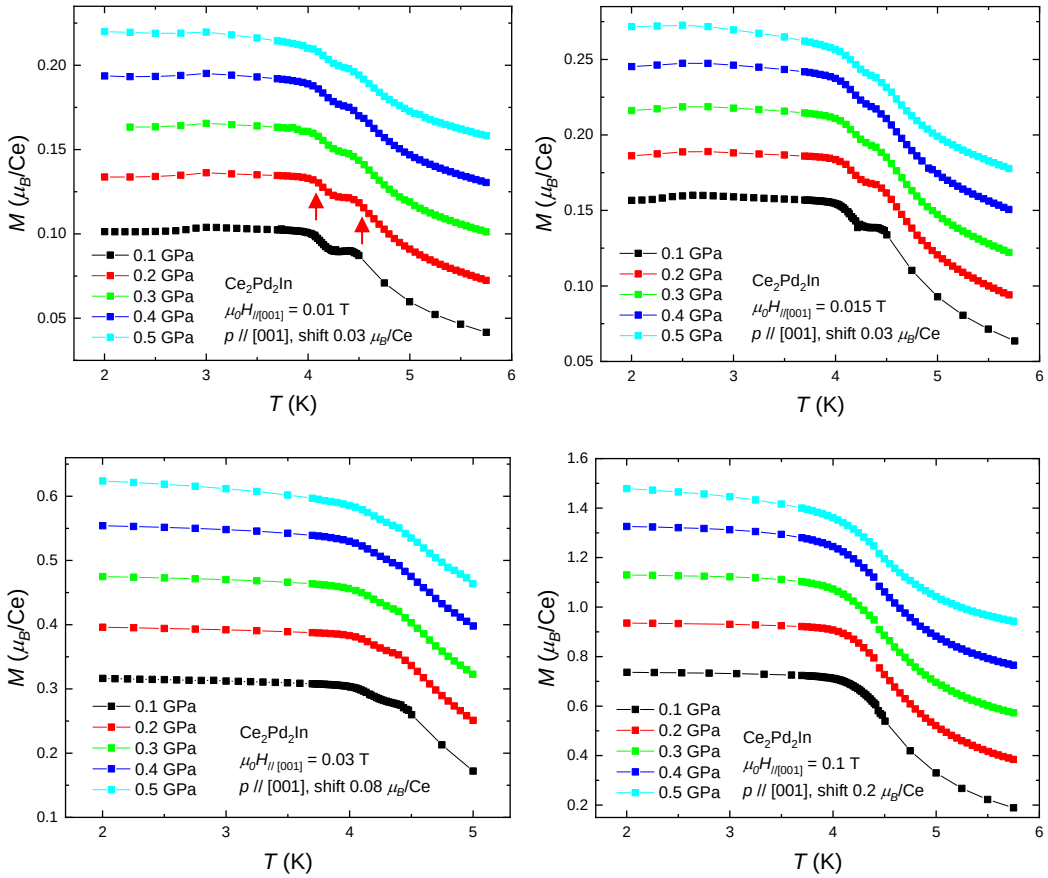

Figure 18: Temperature dependence of magnetization under the influence of uniaxial pressure and various values of external magnetic field, curves were shifted for higher lucidity by the value mentioned in each graph. As an example, the positions of transitions (inflex points) are marked by the arrows on one curve.

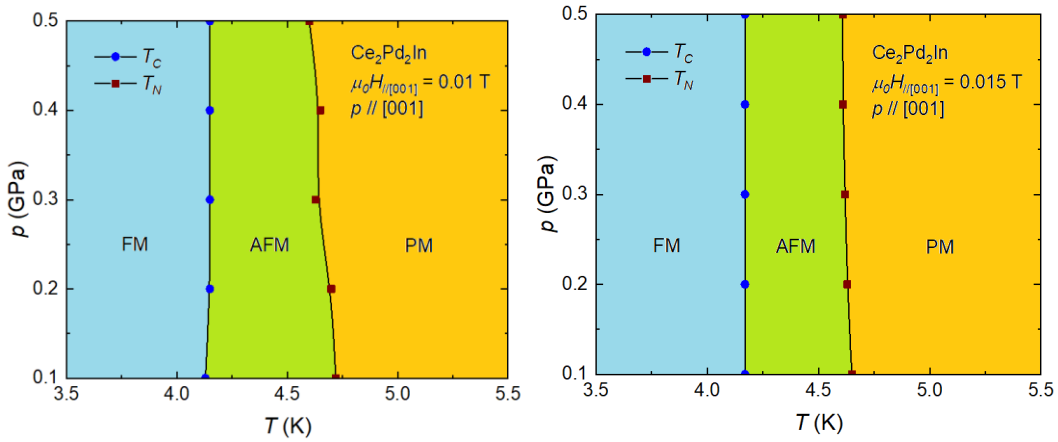

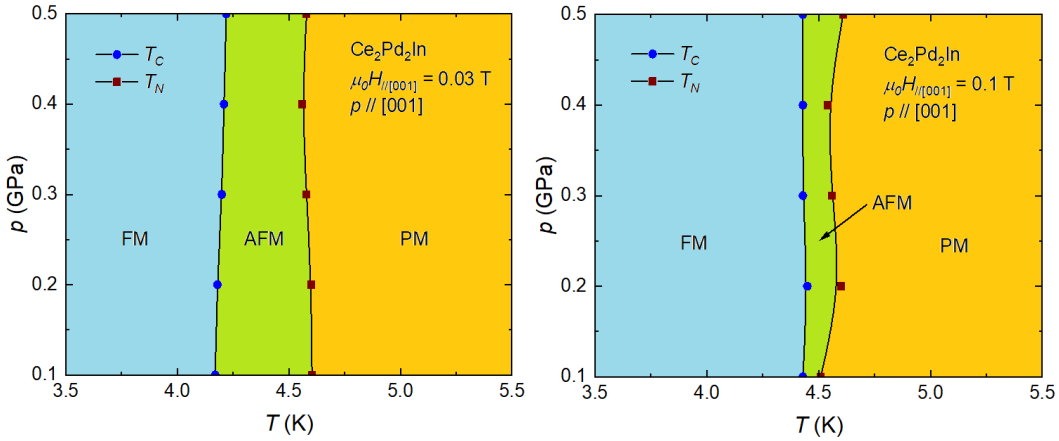

Figure 19: Uniaxial p - T phase diagrams of Ce_2Pd_2In. FM stands for the ferromagnetic, AFM for antiferromagnetic and PM for paramagnetic region.

The magnetization curves measured in uniaxial pressure and the temperature of 2 K are shown in Figure 21. Magnetization reaches the saturation quickly and we can see that the saturation value of magnetization is decreasing with increasing the uniaxial pressure. The behavior of saturated magnetization is similar to the hydrostatic pressure case, but the effect of uniaxial pressure is larger. The saturation at $p_{uniaxial} = 0.4$ GPa is near the value obtained for $p_{hydrostatic} = 0.8$ GPa, μ_{sat} reached at $p_{uniaxial} = 0.5$ GPa is much lower than the value found for the highest applied hydrostatic pressure 1.1 GPa.

In higher magnetic fields, the decreasing tendency of the curves measured in the pressure was observed. This is caused by the diamagnetic contribution of the pressure cell originating in the CuBe alloy and other components of the pressure cell. The diamagnetic contribution to the total magnetization is significant in higher fields, where the moment of Ce is constant. That's why the correction was done and the contribution of pressure cell was subtracted. Data in the following have been already recalculated.

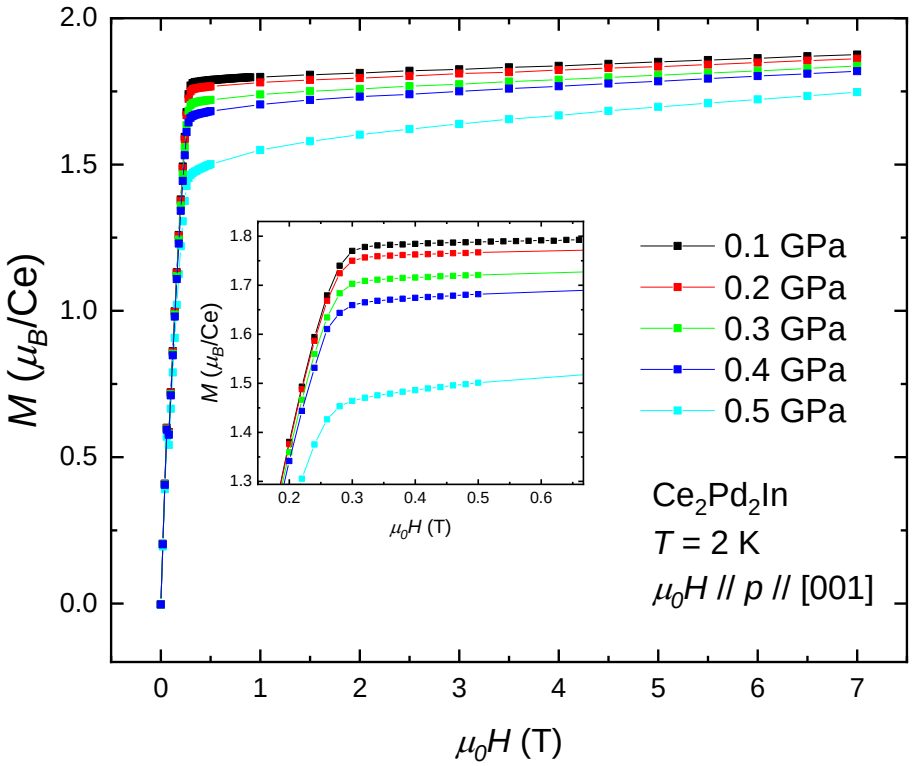

Figure 20: Magnetization curves measured in uniaxial pressure

Discussion

Measurements of transport and magnetic properties were carried out on single-crystalline sample of the prism-like shape with the longest dimension along crystallographic *c*-axis and with shorter dimensions oriented along [110]. Our research is the continuation of systematic study of Ce_2Pd_2In compound. The sample used for our study originates from the same Czochralski crystal growth as the samples discussed by Klicpera et al. [24], which allows us to take into account the previous results, compare and verify our measurements. However, some differences were found, which will be discussed below.

The X-ray powder diffraction was carried out on powder polycrystalline sample and revealed strong anisotropy of crystal lattice temperature evolution. The diffraction pattern was analyzed, and indices of all peaks were can be ascribed to P4*/mbm* space group. However, one peak present at the angle $2\theta = 103.5°$ cannot be attributed to the diffraction on studied crystal. It originates from the diffraction on saphire which is used in the diffractometer as the pad for the sample.

Temperature dependence of crystal lattice provides the information about evolution of distances between the nearest magnetic neighbors. The distance between Ce atoms in our case is responsible for the resulting magnetic properties. The most typical exchange interaction for 4f intermetallic systems is RKKY interaction, which strongly depends on the distance between magnetic ions. As it has been already mentioned above, in whole temperature region from room temperature down to 3.2 K, the nearest magnetic neighbors are lying in the basal plane. On the other hand, the distance between Ce ions in different lattice plane sheets (the second nearest neighbors) is longer and the difference between these two distances is getting more significant with decreasing temperature. We can say that the basal-plane lattice parameters are softer than parameter *c* with respect to the temperature influence because the changes of *c* are approximately two times smaller than that of *a*. It is typical that the same trend will be present also under pressure, so we can expect that the hydrostatic pressure will affect more the basal direction than *c*-axis. It inspired us to carry out also the uniaxial pressure experiment with pressure applied along *c*-axis.

All experiments provide information about magnetic phase transitions. The accurate position was determined from the heat capacity data using the method of idealization of transition according to specific heat while maintaining the entropy. The positions at ambient pressure and magnetic field were determined as $T_C = 4.16\,\mathrm{K}$ and $T_N = 4.65\,\mathrm{K}$. At these temperatures, the magnetization curve and the curve of AC magnetic susceptibility exhibit the inflex points which can be further used for determination of positions of the transitions. On the resistivity data, we can also observe two anomalies corresponding to the phase transitions, but they are lying at temperatures below the actual positions of transitions.

The shape of obtained curves and also the values are in good agreement with the previously published data.

Investigating of critical temperatures allowed us to construct the phase diagrams. Even in low magnetic fields below 0.05 T, the anomalies corresponding to individual phase transitions are merging and the ferromagnetic order is reached at higher temperature.

Impact of the pressure is very interesting. The external hydrostatic pressure affects both observed transitions, however the changes in the Néel temperature is not as

significant and systematic as in case of the Curie temperature. Under applied pressure, T_C is shifted down to the lower temperatures. Extension of the experiment to higher pressure range is needed to estimate total suppression of ferromagnetic phase. Expected pressure needed for the suppression – approximately 5 GPa – was estimated from the extrapolation of the phase diagram. This pressure range can be reached in our laboratory conditions and remains as the subject for further investigation.

The fact that the ferromagnetic phase is being suppressed may be the effect of general trend of pressure suppressing of all form of magnetism in solids. The pressure leads generally to the higher overlap of atomic wave functions and stronger bonds. This itinerant behavior is inconsistent with present of magnetism requiring localized behavior [7,9].

On the other hand, the uniaxial pressure applied along *c*-axis does not affect the positions of magnetic transitions significantly up to the highest applied pressure of 0.5 GPa. The uniaxial pressure allows us to directly influence the lattice parameters along the particular direction. We used the pressure applied along the direction which is more rigid with respect to temperature effect. The pressure applied along this direction acts against the fact that the nearest magnetic neighbors are lying in the basal plane. It is not possible to say (due to the experimental limits) what happens with basal plane interatomic distances under the influence of uniaxial pressure applied along *c*. It is possible that the main role plays the tendency to keep the volume – in such case the basal plane is growing, or the tendency to keep the symmetry – than the ratio between the interatomic distances remains the same in all pressures. These two scenarios can be described by different Poisson ratio of the compound with nonzero value in the first case and zero value for the constant *a*. Usual metallic materials show Poisson ratio around 0.3 and for example of almost zero Poisson ratio we can mention cork [29]. The first mentioned scenario can explain the differences in phase diagrams observed at hydrostatic and uniaxial pressure, where the uniaxial pressure does not suppress the ferromagnetic phase on the contrary to the hydrostatic one. If it is truth that the evolution of lattice with pressure is similar to that with decreasing temperature, we can expect that the Ce atoms lying in the same basal plane which represents the nearest magnetic neighbors are getting even closer under influence of hydrostatic pressure.

This can lead to the increase of antiferromagnetic interaction and thus to suppression of ferromagnetic phase.

Another feature observed both in hydrostatic and uniaxial pressure is the suppression of saturated magnetic moment. Here is the effect of uniaxial pressure significantly stronger than that of the hydrostatic one. This effect is probably caused by pressure induced increase of magnetic fluctuations in studied system and is in agreement with the increase of the value of residual resistivity.

Conclusion

This thesis is focused on the study of physical properties of selected rare earth element-based compound Ce_2Pd_2In. Detailed ambient pressure characterization in terms of lattice, electric, magnetic and thermal properties was carried out on the single crystalline sample. The main aim of the thesis was to investigate the pressure influence on physical properties. Three types of pressure cells allowing us to measure electric and magnetic properties were used to apply the hydrostatic pressure up to 3 GPa and also the uniaxial pressure up to 0.5 GPa.

In terms of the crystal structure study, the belonging to the tetragonal structure with space group P4/*mbm* was verified and the room temperature lattice parameters were found to be $a = 7.801(2)$ Å and $c = 3.919(1)$ Å. The temperature evolution of lattice parameters exhibits strong anisotropy, the evolution of the volume of unit cell is driven mainly by *a*, which is decreasing with decreasing temperature. On the other hand, *c* is increasing, but its changes are smaller.

The phase transitions manifest themselves as the inflex points on the magnetization curves and on AC magnetic susceptibility data. It allows us to construct the phase diagram. We can see that even small external magnetic field (lower than 0.05 T) leads to suppression of antiferromagnetic phase.

Application of hydrostatic mechanical pressure leads to lowering of the saturated value of magnetization due to the magnetic fluctuations and it also significantly influence the temperatures of magnetic phase transitions, especially the Curie temperature is shifted to the lower temperatures and the antiferromagnetic region is being broadened. The pressure evolution of Néel temperature is not so significant.

As for the uniaxial pressure applied along [001], the lowering of saturated magnetic moment is even more significant. On the other hand, the positions of phase transitions are not affected a lot.

Bibliography

[1] Shah K. V. et al., *The $Yb_2Al_{1-x}Mg_xSi_2$ series from a spin fluctuation (x=0) to a magnetically ordered ground state (x=1).* Journal of Physics: Condensed Matter 2009, 21 (17), 6001.

[2] Patil S. et al., *Anomalies of resistivity and its T3-dependence at low temperatures in Eu-based valence fluctuating systems*. Solid state communications 1990, *76* (10), 1173-1176.

[3] Wohlleben D., Wittershagen B., *Resistivity anomalies due to valence fluctuations.* Advances in Physics 1985, 34 (3), 403-443.

[4] Sales B. C., Wohlleben D., *Susceptibility of interconfiguration-fluctuation compounds*. Physical Review Letters 1975, 35 (18), 1240-1244.

[5] Gumeniuk R. et al., *Valence fluctuations of europium in the boride $Eu_4Pd_{29+x}B_8$.* Journal of Physics-Condensed Matter 2016, *28* (11), 9.

[6] Iwasieczko W., Kaczorowski D., *Hydrogen insertion effect on the magnetic properties of Ce_2Pd_2In.* Journal of Alloys and Compounds 2011, *509* (5), 1384-1388.

[7] Ashcroft N. W., Mermin N. D., *Solid state physics.* Saunders College Publishing, Philadelphia, 1976.

[8] Arnold Z., *High pressure in basic and material science*. Lecture notes.

[9] Prchal J., Arnold Z., Sechovský V., Fyzika ve vysokých tlacích, prezentace k přednášce.

[10] Bireckhoven B., Wittig J., *A diamond anvil cell for the investigation of superconductivity under pressures of up to 50 GPa: Pb as a low temperature manometer*. Journal of Physics E: Scientific Instruments 1988, *21* (9), 841.

[11] Fujiwara N. et al., *Fabrication and efficiency evaluation of a hybrid NiCrAl pressure cell up to 4 GPa*. Review of Scientific Instruments 2007, 78 (7), 073905.

[12] *Pressure cells*, [online]. Material Properties Measurement Laboratory, Materials Growth and Measurement Laboratory. Available on https://mgml.eu/.

[13] Wikipedia Contributors, Black garden ant, [online]. Wikipedia, the free encyclopedia, 19.5.2020, Last change 17.5.2020. Available on https://en.wikipedia.org/wiki/Black_garden_ant

[14] Murata K. et al., *Pressure transmitting medium Daphne 7474 solidifying at 3.7 GPa at room temperature*. Review of Scientific Instruments 2008, 79 (8), 085101.

[15] Staško D., *Pressure media for high pressure experiments, the family of Daphne*. To be published.

[16] Kamarád J. et al., *High pressure cells for magnetic measurements – Destruction and functional tests*. Review of Scientific Instruments 2004, 75, 5022.

[17] Yokogawa K. et al., *Solidification of high-pressure medium Daphne 7373*. Japanese journal of applied physics 2007, 46, 3636.

[18] Kamarád J. et al., *Miniature uniaxial pressure cells for magnetic measurements*. High Pressure Research 2008, 28, 633.

[19] Lukachuk M., Pöttgen R., *Intermetallic compounds with ordered U_3Si_2 or Zr_3Al_2 type structure–crystal chemistry, chemical bonding and physical properties.* Zeitschrift für Kristallographie-Crystalline Materials 2003, 218 (12), 767-787.

[20] Ye L., *Electronic transport on the Shastry-Sutherland lattice in Ising-type rare-earth tetraborides*. Physical Review B 2017, 95 (17), 174405.

[21] Kaczorowski D. et al., *Magnetic behavior in a series of cerium ternary intermetallics: Ce_2T_2In (T=Ni, Cu, Rb, Pd, Pt, and Au).* Physical Review B 1996, 54 (14), 9891-9902.

[22] Hauser R. et al., *Specific heat and electrical resistivity studies on Ce_2T_2In, T=Ni, Rh, Pt, Pd, Cu and Au*. Physica B 1997, 230, 211-213.

[23] Gordon R. A. et al., *Magnetic properties of several Ce(2)T(2)M phases with T=Ni, Pd and M=In, Sn, Pb*. Journal of Alloys and Compounds 1995, 224(1), 101-107.

[24] Klicpera M. et al., *Magnetic properties of Czochralski-grown Ce_2Pd_2In single crystal.* Journal of Magnetism and Magnetic Materials 2016, 404, 250-256.

[25] Herrmannsdörfer T. et al., *Magnetic ordering in the rare-earth intermetallic compounds Tb_2Pd_2In and Ho_2Pd_2In.* Physica B: Condensed Matter 2000, 276, 702-703.

[26] Fischer P., *Antiferromagnetic rare-earth ordering in the intermetallic compounds R_2Pd_2In (R= Pr, Nd).* Journal of Physics: Condensed Matter 2000, 12 (31), 7089.

[27] Braghta A. et al., *Magnetic and thermal properties of Ce2Pd2Sn.* Journal of magnetism and magnetic materials 2008**,** *320* (6), 1141-1145.

[28] Giovannini M. et al., *Effect of nonstoichiometry on the transition from ferromagnetism to antiferromagnetism in the ternary indides $Ce_{1.95}Pd_{2+2x}In_{1-x}$ and $Ce_{2+x}Pd_{1.85}In_{1-x}$.* Physical Review B 2000, 61 (6), 4044-4053.

[29] Fortes M. A., Nogueira M. T., *The Poisson Effect in Cork*. Materials Science and Engineering 1989, A122, 227-232.